Proc. Natl. Acad. Sci. USA
Vol. 91, pp. 5652–5656, June 1994
Biophysics

Finding a needle in a haystack: Detection of a small protein (the 12-kDa VP26) in a large complex (the 200-MDa capsid of herpes simplex virus)

F. P. BOOY*, B. L. TRUS*†, W. W. NEWCOMB‡, J. C. BROWN‡, J. F. CONWAY*, AND A. C. STEVEN*§

*Laboratory of Structural Biology, National Institute of Arthritis, Musculoskeletal and Skin Diseases, and †Computational Bioscience and Engineering Laboratory, Division of Computer Research and Technology, National Institutes of Health, Bethesda, MD 20892; and ‡Department of Microbiology and Cancer Center, University of Virginia Health Sciences Center, Charlottesville, VA 22908

Communicated by Henry Metzger, March 25, 1994 (received for review January 12, 1994)

ABSTRACT **Macromolecular complexes that consist of homopolymeric protein frameworks with additional proteins attached at strategic sites for a variety of structural and functional purposes are widespread in subcellular biology. One such complex is the capsid of herpes simplex virus type 1 whose basic framework consists of 960 copies of the viral protein, VP5 (149 kDa), arranged in an icosahedrally symmetric shell. This shell also contains major amounts of three other proteins, including VP26 (12 kDa), a small protein that is approximately equimolar with VP5 and accounts for ≈6% of the capsid mass. With a view to inferring the role of VP26 in capsid assembly, we have localized it by quantitative difference imaging based on three-dimensional reconstructions calculated from cryo-electron micrographs. Purified capsids from which VP26 had been removed *in vitro* by treatment with guanidine hydrochloride were compared with preparations of the same depleted capsids to which purified VP26 had been rebound and with native (undepleted) capsids. The resulting three-dimensional density maps indicate that six VP26 subunits are distributed symmetrically around the outer tip of each hexon protrusion on VP26-containing capsids. Because VP26 may be readily dissociated from and reattached to the capsid, it does not appear to contribute significantly to structural stabilization. Rather, its exposed location suggests that VP26 may be involved in linking the capsid to the surrounding tegument and envelope at a later stage of viral assembly.**

A general organizing principle in supramolecular assembly is for a complex to consist of a structural framework that is a polymer of a basic building block—often a single protein species—with other proteins attached at certain specific sites. These additional proteins may regulate the assembly process, modulate the stability of the complex, link it to other structures, or otherwise confer functional specificity. Examples of such complexes abound in the cytoskeleton, the extracellular matrix, biological membranes, and many kinds of viruses.

Herpesviruses are among the most genetically complex of animal viruses. The large sizes [120–230 kbp (1)] of their double-stranded DNA genomes are reflected in the dimensions and structural complexity of their capsids. The herpes simplex virus type 1 (HSV-1) capsid, ≈125 nm in diameter, has an icosahedral triangulation number of 16 (2). Its surface shell is 15 nm thick and is made up of 12 pentons and 150 hexons (3) whose most prominent features are hollow cylindrical protrusions that extend ≈5 nm outward beyond the rest of the shell. Protein nodules called "triplexes" (4) are present at the sites of local threefold symmetry and are surrounded by triplets of capsomer protrusions. The innermost layer of the shell is a continuous 4-nm-thick sheet of protein that is interrupted only by the openings of the channels that pass axially through each of the 162 capsomers. This structure is common to purified B capsids (a DNA-free precursor), DNA-filled C capsids, and empty A capsids (5–8).

Unlike the capsids of simpler viruses, which are often polymers of a single protein species, the HSV capsid shell contains four proteins in major amounts. VP5 (149 kDa; 960 copies) forms the basic icosahedral matrix and assumes conformationally and antigenically distinct forms at the penton and hexon sites (7, 8). VP19 (50 kDa; ≈350 copies) and VP23 (35 kDa; ≈550 copies) are thought to make up the triplexes (8) and may play a stabilizing role. The fourth capsid protein, VP26 [12 kDa; ≈1000 copies (8, 9) and of basic charge (10)], has not been localized nor has its functional significance been established. Mapping of VP26 would complete the interpretation of the structural features of the capsid shell in terms of its molecular constituents. In the present study, we used quantitative difference imaging (8, 11–14) to accomplish this localization. Our experiments were designed to exploit the observations (15) that (*i*) treatment of native HSV-1 B-capsids with 2.0 M guanidine hydrochloride solubilizes VP26 while leaving the residual capsids (called G2.0 capsids) largely intact and (*ii*) purified VP26 may subsequently rebind to them, producing "G26 capsids." Thus our goal was to detect structural differences between G26 capsids and G2.0 capsids and relate them to the presence or absence of VP26.

MATERIALS AND METHODS

Production and Characterization of G2.0 Capsids and G26 Capsids. Previously described procedures (8, 15, 16) were employed for purifying HSV-1 B capsids from infected BHK-21 cells and for converting them into G2.0 capsids by extraction *in vitro* with 2.0 M guanidine hydrochloride. To isolate VP26, 200–300 μl of purified B capsids at ≈1.5 mg/ml in TNE (0.5 M NaCl/1 mM EDTA/20 mM Tris·HCl, pH 7.5) was immersed in a water bath and heated by slowly raising the bath temperature until the capsids precipitated; this occurred between 55°C and 65°C. The precipitate was removed by low-speed centrifugation (1000 × *g*), and the supernatant contained solubilized VP26. To produce G26 capsids, 200–300 μl of VP26 prepared as described above was mixed with 100 μl of G2.0 capsids (at 1.0 mg/ml in TNE), corresponding to a VP26/VP5 molar ratio of ≈2.5. The sample was incubated for 1 hr at room temperature, and the resulting G26 capsids were separated from unbound VP26 by centrifugation on a 5-ml linear 20–40% (wt/vol) sucrose

The publication costs of this article were defrayed in part by page charge payment. This article must therefore be hereby marked "*advertisement*" in accordance with 18 U.S.C. §1734 solely to indicate this fact.

Abbreviation: HSV-1, herpes simplex virus type 1.

§To whom reprint requests should be addressed at: Laboratory of Structural Biology, National Institute of Arthritis, Musculoskeletal, and Skin Diseases, Building 6, Room 425, National Institutes of Health, Bethesda, MD 20892.

gradient (prepared in TNE) for 45 min at 24,000 rpm in a Beckman SW50.1 rotor operated at 4°C. G26 capsids (the only visible light-scattering band) were removed from the gradient and concentrated by centrifugation through a layer of 20% sucrose (17). The protein composition of capsids and VP26 preparations was determined by SDS/PAGE followed by Coomassie blue staining (8, 16). The pyridine dye elution method (18) was used to determine the amount of VP26 present (relative to the amount of VP5) in B and G26 capsids, by taking into consideration the reduced amount of VP5 per capsid in G26 capsids and G2.0 capsids (8) due to their loss of pentons.

Cryo-Electron Microscopy. Capsid preparations at 1–2 mg of protein per ml were prepared for cryo-electron microscopy and observed as described (6). Micrographs were recorded at a nominal magnification of ×36,000, by using low-dose techniques, on a Philips EM400T equipped with a Gatan (Warrendale, PA) model 626 cryoholder and modified Gatan anticontamination blades. The microscope was operated under standard conditions throughout these experiments.

Image Processing and Three-Dimensional Reconstruction. Micrographs were screened by optical diffraction to identify images with defocus values such that the first zero of the phase-contrast transfer function was at ≈1/(2.5 nm). Two such micrographs of G2.0 capsids and two of G26 capsids were selected and digitized on a Perkin–Elmer 1010MG microdensitometer at a sampling rate of ≈0.83 nm per pixel. Reconstructions were calculated by "common lines" techniques of Fourier analysis (19–21, 37) as described (6, 7), with the preprocessing steps performed using the PIC program (22) and other software that performs the same operations in a more automated manner (23). The computationally intensive programs used to estimate and then to refine the particles' orientations were adapted from code kindly given to us by T. S. Baker (Purdue University) and extensively modified to run on an Intel iPSC/860 massively parallel supercomputer. The Intel versions of these programs are 350–450 times faster than the serial implementation on a VAX 8350, and they have also been modified to provide a user-friendly interface and new refinement options for additional flexibility (C. A. Johnson, personal communication). Each reconstruction was based on data from two micrographs that were independently reconstructed and later combined to include 167 images of G2.0 capsids and 137 images of G26 capsids. The resolution of the final reconstructions was estimated to be ≈3.0 nm in terms of the spatial frequency at which the Fourier ring correlation coefficient dropped to zero (23).

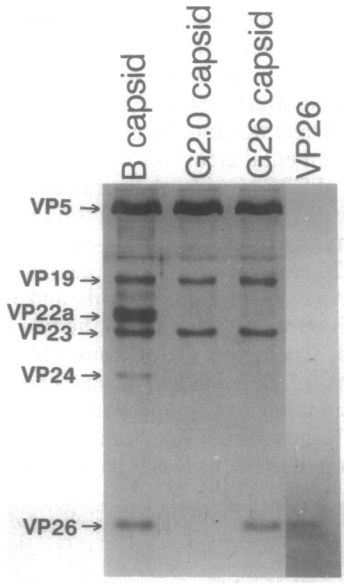

FIG. 1. SDS/PAGE analysis of B capsids, G2.0 capsids, purified VP26, and G26 capsids.

When merging data from different micrographs of such a large particle as the HSV-1 capsid, precise cross-calibration of magnification is essential in order not to compromise the resolution of the resulting density map (24). To perform this operation, a spherically averaged radial density profile was derived from the reconstruction calculated from each micrograph, and a relative scaling factor was determined by carefully matching corresponding features on these profiles. A similar procedure was followed in matching the radial scaling and the relative normalization of density between G2.0 capsids and G26 capsids, whose profiles are essentially superposable, except at the outermost radii (see Fig. 5). The thicknesses of the hexons and pentons were measured from line scans through central sections of the respective reconstructions as the distances between the points on either side at which density fell to background level.

RESULTS

Conversion of G2.0 Capsids to G26 Capsids. Compared with the purified B capsids from which they are derived, G2.0 capsids have lost all of their VP26, 20–30% of their VP19 and

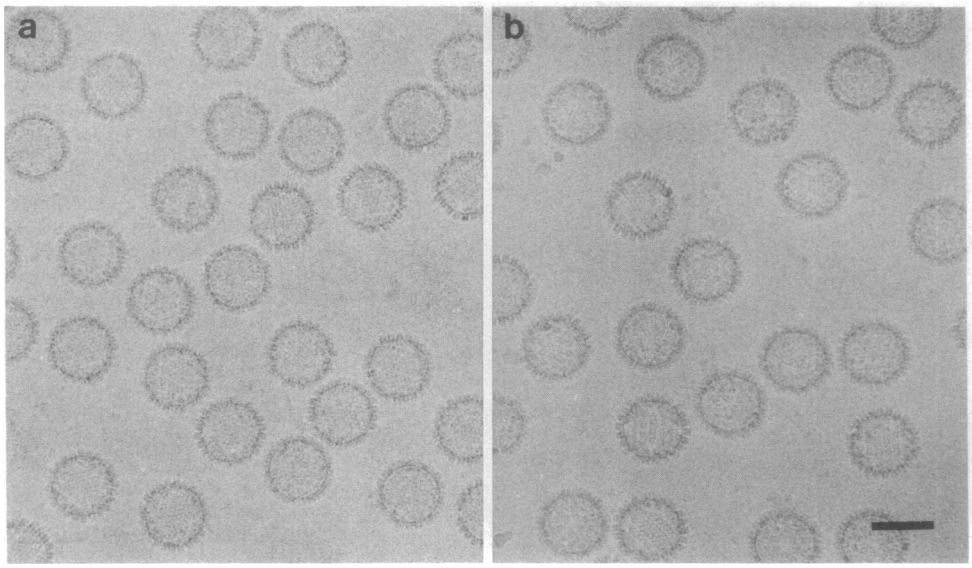

FIG. 2. Cryo-electron micrographs of G2.0 capsids (*a*) and G26 capsids (*b*). These capsid species were generated by *in vitro* manipulations, starting with HSV-1 B capsids purified from infected cells (see ref. 15). (Bar = 100 nm.)

VP23 (the peripentonal triplexes), and ≈6% of their VP5 (the pentons) (8). After incubation with purified VP26, the resulting capsids were found to have rebound VP26 (Fig. 1). Assayed by quantitative SDS/PAGE, the amount of VP26 retained per particle was found to be the same as in B capsids, to within experimental error. VP26 accounts for ≈7% of the particle mass of G26 capsids. A further indication that VP26 had been correctly rebound was that the same concentration of guanidine hydrochloride—1.5 M—was required to extract VP26 from G26 capsids and from B capsids (15).

Structural Analysis of G2.0 Capsids and G26 Capsids. In Fig. 2, cryo-electron micrographs of the two kinds of capsids are compared. There are no obvious differences between them in terms of dimensions or morphological features. Three-dimensional density maps were calculated from these data (Fig. 3). The two reconstructions are largely similar, but close inspection of them, as represented by surface rendering (Fig. 3 *a* and *b*), reveals that the hexon protrusions of G26 capsids are longer than those of G2.0 capsids—i.e., they extend further outward past the level of the triplexes. This conclusion is confirmed in sections (0.83 nm thick) through the respective density maps (Figs. 3 *c* and *d* and 4). At no other sites than the hexon tips is a significant discrepancy observed between G26 capsids and G2.0 capsids.

To further define potential structural differences between them, a three-dimensional difference map was calculated by computational subtraction (Fig. 3 *e* and *f*). The only significant change that it discloses is the one already noted, in which the additional density associated with G26 capsids is localized to six discrete regions, distributed symmetrically around the hexon tips. A similar comparison between G2.0 capsids and B capsids (Fig. 4) revealed the same discrepancy at this site [in addition to previously documented differences elsewhere in the shell (8)].

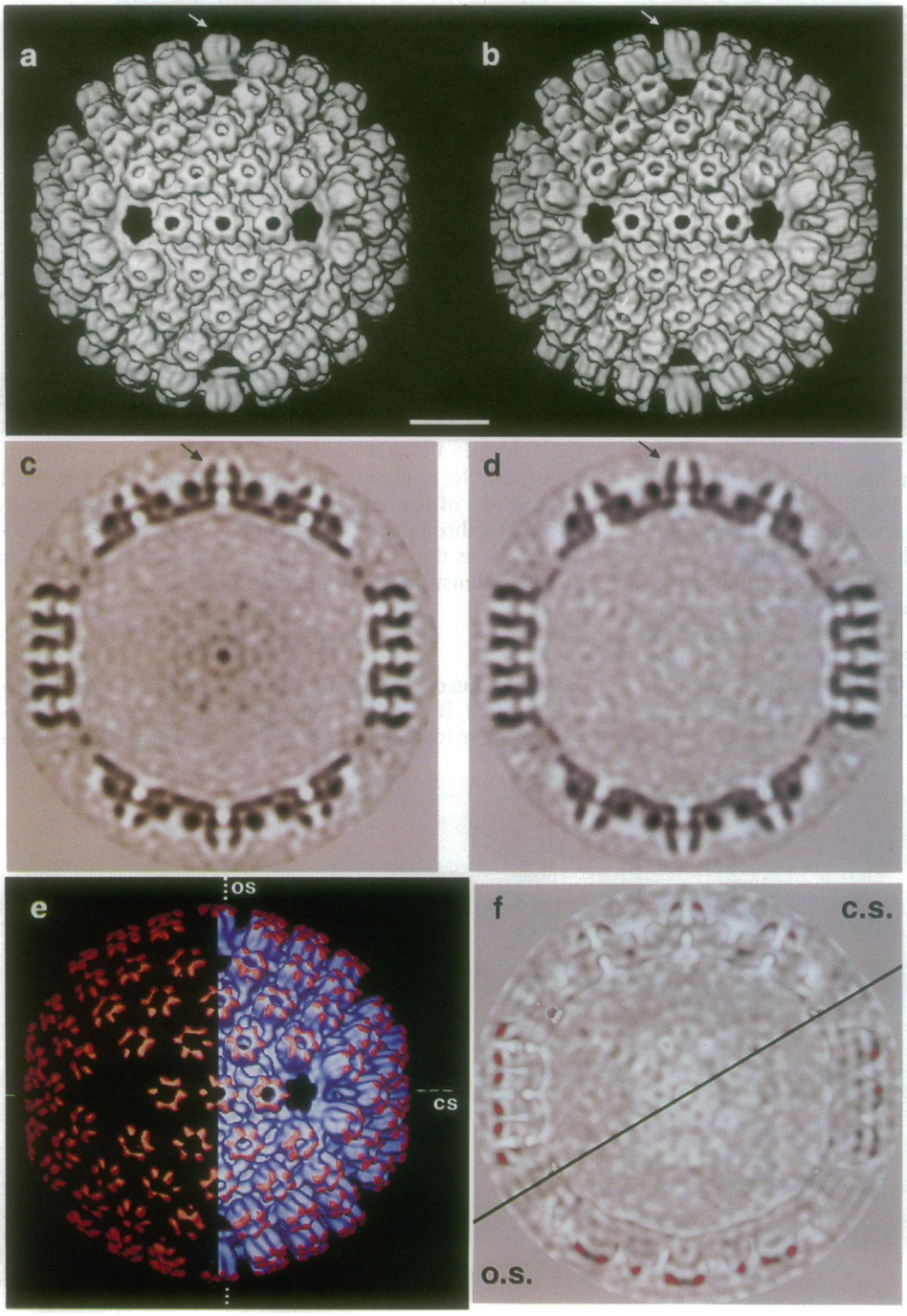

FIG. 3. Comparison between the three-dimensional density maps of G2.0 capsids and G26 capsids, respectively, as represented by surface renderings of the capsids, as viewed along a twofold axis of symmetry (*a* and *b*) and in central sections (0.83 nm thick) perpendicular to this axis (*c* and *d*). Upon conversion to G2.0 capsids, B capsids lose the two sets of triplexes closest to the pentons in addition to their pentons (8). Careful comparison of the triplexes removed in this study with the results of our previous study (8) shows minor differences in the degree of removal of these triplexes. Our experience with these and other batches of G2.0 capsids has been that there is a slight but real variability with respect to this parameter, and as a result we have not been able to fully standardize the experimental procedure. However, the pentons and VP26 are, invariably, completely removed by this procedure. Also shown are difference maps between the two reconstructions (*e Left* and *f*). Densities present in G26 capsids that are not present in G2.0 capsids are coded in red. (*e*) Surface rendering. (*f*) Two 0.83-nm sections through the three-dimensional maps in *e*. The distribution of VP26 alone (*e Left*) and as part of the G26 capsid (*e Right*) is shown. Two sections through the difference map are shown in *f*. In the central thin section (cs), the sectioning plane passes through the six molecules of VP26 that lie along an icosahedral edge (i.e., between vertices) but passes between the VP26 molecules associated with the other hexons sampled by that plane. The latter molecules are detected in an off-centered section (os) that is displaced laterally by 2.5 nm relative to the central section through another twofold axis, perpendicular to the first one. These sectioning planes are marked in *e* by white dotted or dashed lines. (Bar = 25 nm.)

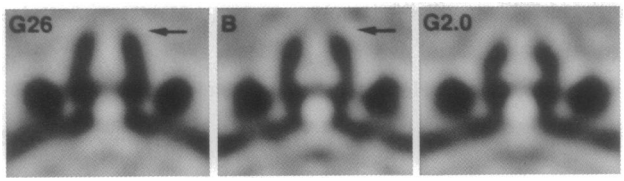

FIG. 4. Central sections through hexons of G26 capsids, B capsids, and G2.0 capsids, as viewed along a twofold axis of symmetry. The hexon protrusions of both G26 capsids and B capsids (arrows) are significantly longer than those of G2.0 capsids, which correlates with the presence or absence of VP26.

The radial density profiles of the two capsid species confirm that they differ only in the presence of this additional outer layer of density, ≈1.8 nm thick, on G26 capsids (Fig. 5).

DISCUSSION

There are several mechanisms whereby multiple protein species may be incorporated into a large complex such as a viral capsid. For instance, they can be generated after assembly by proteolytic processing of precursor polyproteins (e.g., ref. 25), they may first associate into oligomers that serve as the building blocks of the assembling capsid, or additional proteins may bind to sites created by conformational changes of the precursor capsid (e.g., refs. 26 and 27). The capsid of HSV contains four proteins in major amounts—VP5, VP19, VP23, and VP26. They are expressed from separate genes (28), but the details of how they interact during assembly are not yet apparent. In this study, our goal was to complete their localization in the shell of the mature capsid.

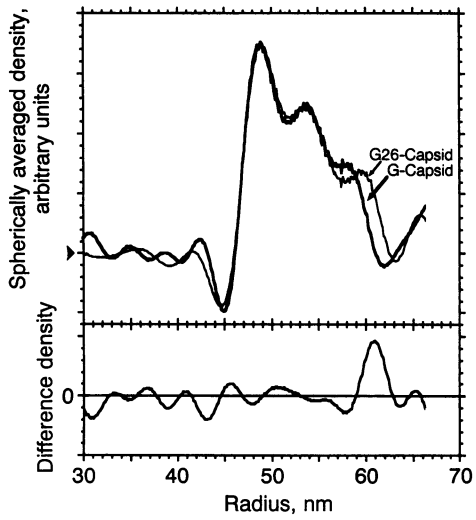

FIG. 5. Spherically averaged radial density profiles were calculated from both of the reconstructions shown in Fig. 3. The spherically averaged capsid shell starts at a radius of ≈46.5 nm and extends to 61 nm (G2.0 capsids) or 63 nm (G26 capsids). The thickness of the VP26-containing shell (15.5–16.0 nm; *Results*) is slightly exaggerated in this profile because of averaging over an icosahedral (not a spherical) structure. The negative dips observed just inside ($r \approx 45$ nm) and, to a lesser extent, just outside the shell are interference fringes arising from the phase-contrast imaging mode. The match between the two profiles is excellent, except between 62 and 64 nm, where additional mass is present on the G26 capsid, as emphasized in the difference curve at the bottom. *A priori*, our results could have been affected by differential compression of the capsids in ice layers of different thickness. These profiles provide strong evidence against such an eventuality, which would be expressed in the reconstructions as radial smearing to different extents. The exact match of the profiles between radii of 46 nm and 58 nm indicates that either flattening did not occur to a significant extent or that it affected both reconstructions equally.

Location of VP26. Our results imply that the additional density present at the hexon tips of G26 capsids and B capsids, compared with G2.0 capsids, marks the location of VP26. The subunits visualized in the difference map (Fig. 3*e*) should be monomers, to account for the known copy number of VP26 (8). In principle, the observed structural difference at the hexon tips could also be generated allosterically by VP26 binding to some remote site on the capsid surface and transmitting a signal for a structural rearrangement in the tip region. However, it appears unlikely that VP26 could be added without some discernible structural change also taking place at its binding site. Since we see no evidence for any significant changes other than at the hexon tips, we view this latter hypothesis as improbable.

In our previous comparison between B capsids and G2.0 capsids (8), we were not able to correlate any structural difference with the absence of VP26 from G2.0 capsids. That we have been able to map this protein in the present study is attributable to two factors: (*i*) By refining the orientation angles and origins of larger numbers of capsids on a parallel computer, we were able to achieve density maps with considerably higher signal-to-noise ratios and slightly higher resolution than the previous G2.0 capsid map (8). In consequence, the positive density detected at the hexon tips exceeded residual noise fluctuations anywhere else in the difference map. (*ii*) Difference mapping between G26 and G2.0 capsids could be conducted without the distraction of the other more-pronounced structural changes that occur when B capsids are converted to G2.0 capsids (see above).

Penton Sites. Because G2.0 capsids do not contain pentons, we are unable to answer directly the question of whether VP26 is also present at their tips. The appreciable difference in thickness between hexons with and without VP26—15.8 and 14.0 nm, respectively—suggests that penton thickness may offer a clue. Thus, the measured thickness of pentons (≈15.6 nm) suggests that their tips may also contain VP26. However, the conformational differences that have been observed between VP5 as deployed in pentons and hexons, respectively (7, 8), argue that this issue should be settled by a more direct approach.

At an earlier stage of this study, G2.0 capsids were complemented with the proteins solubilized from B capsids by the guanidine hydrochloride treatment instead of with purified VP26. The resulting capsids, which had reacquired VP26, were found to show a build-up of density at their vacated penton sites, although different in form from the original pentons (data not shown). This observation led us to entertain the possibility, among others, that VP26 might form the pentons. In retrospect, this density most likely represented the adhesion of other extracted proteins—either penton-derived VP5 or the internal protein VP22a—to the penton cavities. The pentons have since been shown to be composed largely if not entirely of VP5 (8).

Structure of Tips of Hexon Protrusions. In previous work, we mapped the epitope of monoclonal antibody 8F5 to the tips of hexons (but not of pentons) (7), where our present results also consign VP26. This antibody was raised against purified VP5, and its specificity for VP5 was confirmed by an ELISA assay and has since been corroborated by Western blot analysis (W.W.N. and R. Vasalli, unpublished results). To reconcile these observations, we note that some of the density around the annular tips of hexons—the parts between VP26 subunits (see Fig. 3*e*)—is contributed by VP5. We have been able to localize the centroids of both VP26 (Fig. 3*e*) and the 8F5 epitope (29) quite precisely on the hexon tip, but their boundaries are not sharply defined at our present resolution of 3 nm or so. The situation is further complicated by the

observation that monoclonal antibody 8F5 does not bind efficiently to G2.0 capsids (W.W.N., unpublished results), although it does bind avidly to B capsids (7). It appears, therefore, that the binding of VP26 may influence the conformation of adjacent portions of VP5, including the 8F5 epitope; alternatively, these portions of VP5 may become disordered upon exposure to 2.0 M guanidine hydrochloride.

Functional Implications. The binding of additional proteins to a macromolecular complex can affect its properties in various ways—to stabilize it (e.g., ref. 30), to regulate its size and shape (e.g., ref. 31), or to connect the complex to other molecules or assemblies (e.g., ref. 32). Since VP26 may be removed from HSV-1 capsids without marked effect on their structural integrity, we conclude that this protein does not play an essential role in stabilizing the capsid. Several other possibilities for the function of VP26 are suggested by its localization, each of which yields testable predictions for the phenotypes of mutants defective in its gene, *UL35* (28, 33).

(*i*) VP26 may be dispensible, like bacteriophage T4 capsid protein Hoc (34). This hypothesis anticipates a normal or, at any rate, a significant yield of capsids in *UL35* mutants. In fact, Homa and coworkers (35) have shown that VP26 is at least partially dispensible for capsid assembly. (*ii*) It may have a form-determining or stabilizing function, but only at an early stage of capsid assembly, so that its presence in the mature capsid is extraneous. This hypothesis predicts a reduced yield of correctly formed capsids in *UL35* mutants. (*iii*) A third possibility, suggested by its exposed location, is that VP26 may serve some linkage function. In particular, it may be involved in binding the capsid to the tegument as it proceeds to envelopment. According to this hypothesis, $VP26^-$ capsids would be correctly formed and packaged but should progress out of the nucleus less efficiently than wild-type capsids. Alternatively, it has been proposed that the basically charged VP26 may be involved in the association of preformed capsids with DNA (10, 33). Since the packaged DNA occupies the capsid interior (6), the external location of VP26 is not consistent with interactions between these two constituents in the virion (10), at least on any substantial scale. However, we do not rule out the possibility that VP26 may help to establish an association between precursor capsids and replicating DNA so that packaging may then proceed. This variant predicts a relative accumulation of unpackaged capsids in the nuclei of cells infected with *UL35* mutants.

Localization of Proteins in Other Complexes. In addition to structural entities like virus capsids or cytoskeletal filaments, large complexes play important roles in gene expression, mRNA processing, and signal transduction. Although such complexes do not generally exhibit icosahedral symmetry, the prospects are excellent for localizing protein subunits in them by applying other methods of image reconstruction (e.g., ref. 36) to cryo-electron micrographs. As shown in this study, even small proteins may be unequivocally localized in difference maps at a resolution of 3 nm or so, because the critical determinants are signal-to-noise ratio and contrast, not resolution *per se*. To positively identify molecules, however, it is desirable to complement such a density map with additional information, as with difference mapping or antibody labeling. The most challenging step may well lie in isolating such complexes in biochemically defined states in sufficient quantity for structural analysis.

We are grateful to C. Johnson, N. Weisenfeld, and R. Martino (Division of Computer Research and Technology, National Institutes of Health) for adapting programs to run on the massively parallel Intel iPSC/860 computer and for making this machine available to us. This work was supported in part by National Science Foundation Grant MCB-9119056 to J.C.B.

1. Roizman, B. (1990) in *Virology*, eds. Fields, B. N. & Knipe, D. M. (Raven, New York), pp. 1787–1794.
2. Dargan, D. J. (1986) in *Electron Microscopy of Proteins*, eds. Harris, J. R. & Horne, R. W. (Academic, London), pp. 359–437.
3. Wildy, R., Russell, W. C. & Horne, R. W. (1960) *Virology* **12**, 204–222.
4. Baker, T. S., Newcomb, W. W., Booy, F. P., Brown, J. C. & Steven, A. C. (1990) *J. Virol.* **64**, 563–573.
5. Schrag, J. D., Prasad, B. V., Rixon, F. J. & Chiu, W. (1989) *Cell* **56**, 651–660.
6. Booy, F. P., Newcomb, W. W., Trus, B. L., Brown, J. C., Baker, T. S. & Steven, A. C. (1991) *Cell* **64**, 1007–1015.
7. Trus, B. L., Newcomb, W. W., Booy, F. P., Brown, J. C. & Steven, A. C. (1992) *Proc. Natl. Acad. Sci. USA* **89**, 11508–11512.
8. Newcomb, W. W., Trus, B. L., Booy, F. P., Steven, A. C., Wall, J. S. & Brown, J. C. (1993) *J. Mol. Biol.* **232**, 499–511.
9. Newcomb, W. W., Brown, J. C., Booy, F. P. & Steven, A. C. (1989) *J. Virol.* **63**, 3777–3783.
10. McNabb, D. S. & Courtney, R. J. (1992) *J. Virol.* **66**, 4939–4847.
11. Aebi, U., van Driel, R., Bijlenga, R. K., ten Heggeler, B., van den Broek, R., Steven, A. C. & Smith, P. R. (1977) *J. Mol. Biol.* **110**, 687–698.
12. Carrascosa, J. L. & Steven, A. C. (1978) *Micron* **9**, 199–206.
13. Dryden, K. A., Wang, G., Yeager, M., Nibert, M. L., Coombs, K. M., Furlong, D. B., Fields, B. N. & Baker, T. S. (1993) *J. Cell Biol.* **122**, 1023–1041.
14. Yeager, M., Berriman, J. A., Baker, T. S. & Bellamy, A. R. (1994) *EMBO J.* **13**, 1011–1018.
15. Newcomb, W. W. & Brown, J. C. (1991) *J. Virol.* **65**, 613–620.
16. Newcomb, W. W. & Brown, J. C. (1989) *J. Virol.* **63**, 4697–4702.
17. Newcomb, W. W. & Brown, J. C. (1994) *J. Virol.* **68**, 433–440.
18. Fenner, C., Traut, R. R., Mason, D. T. & Wikman-Coffelt, J. (1975) *Anal. Biochem.* **63**, 595–602.
19. Fuller, S. D. (1987) *Cell* **48**, 923–934.
20. Baker, T. S., Drak, J. & Bina, M. (1988) *Proc. Natl. Acad. Sci. USA* **85**, 422–426.
21. Baker, T. S., Drak, J. & Bina, M. (1989) *Biophys. J.* **55**, 243–253.
22. Trus, B. L., Unser, M., Pun, T. & Steven, A. C. (1992) *Scanning Microsc. Suppl.* **6**, 441–451.
23. Conway, J. F., Trus, B. L., Booy, F. P., Newcomb, W. W., Brown, J. C. & Steven, A. C. (1993) *J. Struct. Biol.* **111**, 222–223.
24. Aldroubi, A., Trus, B. L., Unser, M., Booy, F. P. & Steven, A. C. (1992) *Ultramicroscopy* **46**, 175–188.
25. Molla, A., Paul, A. V. & Wimmer, E. (1991) *Science* **254**, 1647–1651.
26. Steven, A. C., Couture, E., Aebi, U. & Showe, M. K. (1976) *J. Mol. Biol.* **106**, 187–221.
27. King, J. (1980) in *Biological Regulation and Development*, ed. Goldberger, R. F. (Plenum, New York), pp. 101–132.
28. Davison, M. D., Rixon, F. J. & Davison, A. J. (1992) *J. Gen. Virol.* **73**, 2709–2713.
29. Steven, A. C., Newcomb, W. W., Booy, F. P., Brown, J. C. & Trus, B. L. (1992) in *Proceedings of the 50th Annual Meeting of the Electron Microscopy Society of America* (San Francisco Press, San Francisco), pp. 522–523.
30. Ross, P. D., Black, L. W., Bisher, M. E. & Steven, A. C. (1985) *J. Mol. Biol.* **183**, 353–364.
31. Way, M. & Weeds, A. (1990) *Nature (London)* **344**, 292–294.
32. Yang, H.-Y., Lieska, N. & Goldman, R. D. (1990) in *Intermediate Filaments*, eds. Goldman, R. D. & Steinert, P. M. (Plenum, New York), pp. 371–391.
33. McNabb, D. S. & Courtney, R. J. (1992) *J. Virol.* **66**, 4839–4847.
34. Ishii, T. & Yanagida, M. (1975) *J. Mol. Biol.* **97**, 655–660.
35. Thomsen, D. R., Roof, L. L. & Homa, F. L. (1994) *J. Virol.* **68**, 2442–2457.
36. Radermacher, M. (1988) *J. Electron Microsc. Tech.* **9**, 359–394.
37. Crowther, R. A. (1971) *Philos. Trans. R. Soc. London B* **261**, 221–230.